How Normalisation Factors Influence the Interpretations of 3D-Printed Sensors for Electroanalysis

Aya Abdalla[1, 2], Fernando Perez[1, 2], Ana Tendero Cañadas[1, 2], Santanu Ray[3] and Bhavik Anil Patel[1, 2*]

[1]School of Pharmacy and Biomolecular Sciences, [2]Centre for Stress and Age-Related Disease and [3]Surface Analysis Laboratory, School of Environment and Technology, University of Brighton, Brighton, East Sussex, UK

*Correspondence should be addressed to Dr Bhavik Patel; Email: b.a.patel@brighton.ac.uk; Tel: +44(0)1273 642418

Highlights

1. 3D printing provides the ability to make electrodes with a vast array of conductive materials
2. Comparison is complex due to varied surface geometry and conductive loads between electrodes
3. Normalisation by eight different approaches showcased varying trends in the behaviour of one electrode to another for three different analytes
4. No single approach of normalisation can be effective for electroanalytical comparison of 3D printed electrodes

Abstract

The ability to produce electrodes through 3D-printing techniques for use in sensing applications has significant potential. This is mainly due to the mass production of electrodes at any desired geometry. However, comparing different 3D-printed carbon electrodes for electroanalytical performance can be challenging due to the significant variation in each conductive printed material. This study investigates different normalisations that could be applied to compare between different 3D-printed electrodes. We compared 3D-printed carbon black and graphene electrodes for the monitoring of three important biological analytes (dopamine, ascorbic acid and hydrogen peroxide). These 3D printed electrodes have different conductive loads and surface profiles, and therefore we utilised eight different approaches for normalising the current response. There was no perfect normalisation technique and therefore using a combination of approaches to survey the best performing electrode would be a better approach. This study showcases the different possible normalisation methods and highlights the impact these can have on the interpretation of electrodes for electroanalytical measurement.

Keywords: 3D-printing, normalisation, graphene, carbon black, dopamine, ascorbic acid, hydrogen peroxide

1. Introduction

Three-dimensional (3D)-printing, also known as additive manufacturing, has been utilised as an approach to produce conductive parts inexpensively, quickly, and with minimum difficulty.[1-7] Studies have shown that carbon black/acrylonitrile butadiene styrene[8], carbon black/polylactic acid (CB/PLA), carbon nanofiber/graphite/polystyrene composite,[9-10] and graphene/polylactic acid (GR/PLA) [11-15] printed electrodes have promise as electrochemical sensors, with potential to monitor various important analytes. Furthermore, this has spurned the development of various novel conductive filaments fabricated commercially and in labs. Filaments such as carbamorph (CB/polycaprolactone),[16] multiwalled carbon nanotubes/polylactic acid,[17] and Cu-Ag nanowires/polycaprolactone [18] have shown large promise in a wide range of sensing applications. However, as a wider range of printable conductive materials become accessible for electrode manufacture, the challenge now is on how to best compare the electroanalytical performance of different 3D-printed electrodes.

Comparison between various electrodes to evaluate the best sensor for electroanalytical measurement is widely conducted, where normalisation is utilised to provide accurate comparison. There are a variety of strategies that have been used to compare between different sensors. These include approaches such as electrochemical active surface area measured using capacitance,[19] geometric surface area, Brunauer-Emmett-Teller surface area, [20] Tafel plots [21] and normalisation of the current response using a known outer-sphere fully reversible redox couple. [22] However, comparison between different 3D-printable filaments poses significant challenges given that sensors often vary by different percentages of conductive material and altered surface geometry due to printing. The ability to compare 3D

printed sensors is far more complex than for sensors made using solid materials such as glassy carbon electrode or screen printed electrodes.

Therefore, this study explores two of the most widely used 3D-printed carbon electrodes, carbon black/polylactic acid and graphene/polylactic acid. These electrodes were compared for the measurement of three extensively measured biological compounds: dopamine (DA), ascorbic acid (AA), and hydrogen peroxide (H_2O_2). The normalisation factors used were geometric surface area, root mean square of height deviation, oxygen functional groups, conductive content, capacitance, resistivity and faradaic current based on both outer and inner sphere redox couples. Utilising these different normalisation factors will lead to a more informed decision into which 3D-printed sensor could have a superior electroanalytical performance for a specific analyte.

2. Materials and Methods

2.1. Reagents

Chemicals used were hexaammineruthenium (III) chloride ($Ru(NH_3)_6^{2/3+}$,98%), potassium ferricyanide(III) ($[Fe(CN)_6]^{2/3-}$, 99%), potassium phosphate monobasic (>99.0%), potassium phosphate dibasic (>98.0%), potassium chloride (>99.0%), dopamine hydrochloride, and L-ascorbic acid (>99.0%), hydrogen peroxide (30% w/w in H_2O), all purchased from Sigma-Aldrich, UK.

2.2. 3D-printing of electrodes and electrochemical pre-treatment

The 3D-printing method was performed as explained previously.[8] Briefly, CB/PLA (Protopasta, WA, USA) and GR/PLA (Black Magic 3D, New York, USA) electrodes

were printed using a Wanhao Duplicator 4 with a 0.4 mm brass nozzle at a bed temperature of 50°C and a nozzle temperature of 200°C for GR/PLA and 220°C for CB/PLA. The infill density was set at 100% along with 2 outer perimeter toolpaths and a layer height of 0.3 mm[23]. The extrusion multiplier was set to 1.1 for this study. All electrodes were printed in a vertical orientation into discs of 3 mm thickness and 10 mm diameter, as our previous studies have indicated that printing orientation has a significant impact in electrochemical performance.[24-25] To achieve this vertical print, the curved face of the disc contained a 5 mm flat section on which it could adhere to the print bed for the build. **Figure 1** shows a light microscopy image of the electrode surface. Following successful printing of these electrodes, they were put into acrylic tubes that were then sealed with Araldite. To obtain an electrical connection, a copper wire was attached to each electrode using CircuitWorks conductive (silver) epoxy. This was then sealed with Araldite, leaving only one flat face of the electrode exposed for testing. The 3D-printed electrodes were electrochemically pre-treated by cycling between -1.5 V and +1.5 V for 2 mins at 0.1 V s^{-1} in a 0.1 M PBS solution at pH 7.4 based on evaluation of previously published studies on these electrodes. [11, 26-29]

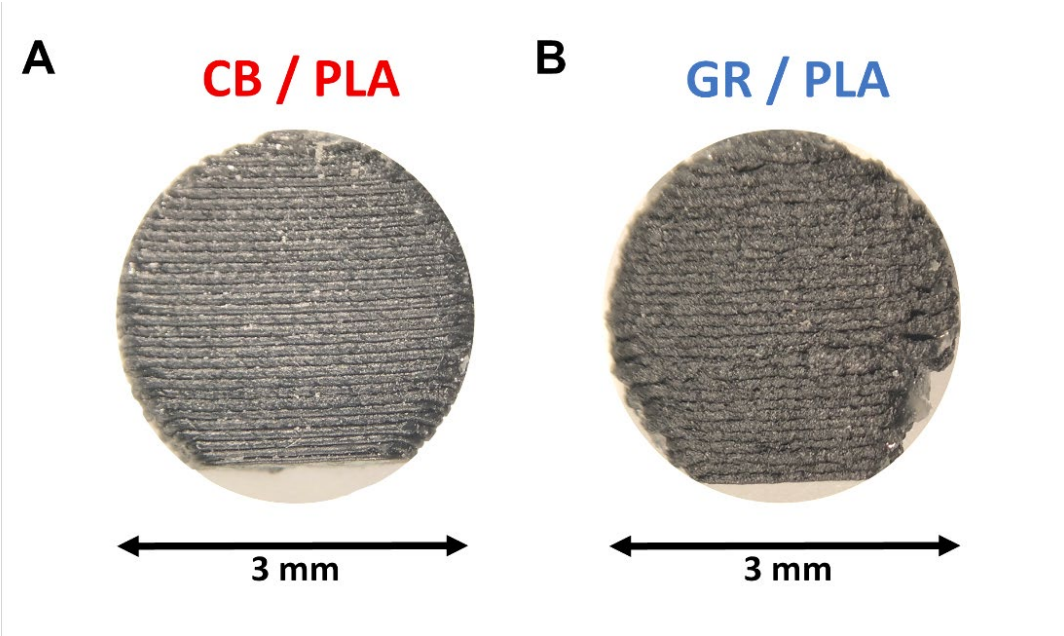

Figure 1. Light microscopy images of (A) CB / PLA and (B) GR / PLA 3D-printed electrodes fabricated in vertical print

2.3. Electrochemical measurements.

Cyclic voltammetry (CV) measurements were carried out on 3D-printed electrodes using a three-electrode system, with the 3D-printed electrodes (surface area of 78.5 mm^2) as the working electrode, a platinum wire as the auxiliary electrode and Ag/AgCl (3.0 M KCl) as the reference electrode. All experiments were carried out using a CHI 760E potentiostat (CHI Instruments, TX, USA).

Capacitance measurements were carried out by CV (same three electrode system as above) in 0.5 M KCl over a potential window of + 0.2 V to - 0.2 V at a scan rate of 0.1 V s^{-1}, and calculations were carried out at 0 V. To calculate the average capacitance for each electrode, the sum of the absolute values of the anodic and cathodic currents at 0 V were calculated and divided by two times the scan rate. [30]

1 mM $Ru(NH_3)_6^{2+/3+}$ and 1mM $[Fe(CN)_6]^{2/3-}$ were prepared in 0.5 M KCl while 1 mM of DA and AA were both prepared in 0.1 M phosphate buffer at pH 7.4. The wave form for $Ru(NH_3)_6^{2+/3+}$ was 0.2 V to -0.5 V, for $[Fe(CN)_6]^{2/3-}$ the potential window was 0.0 V to 0.6 V, while the potential window for both DA and AA were -0.2 V to 0.6 V. All potential window were performed at a scan rate of 0.1 V s^{-1}. For all electrochemical measurements 10 cycles were completed for each electrode at a scan rate of 0.1 V s^{-1} and 3 electrode replicates were used for all experiments.

Peroxide calibration was carried out by amperometry at 0.5 V with continuous stirring. Increasing concentrations (between 0.5 mM and 15 mM) of peroxide in 0.1 M PBS were injected at 100 s interval post baseline stabilization.

2.4. Scanning electron microscopy (SEM)

The samples were imaged using a Zeiss SIGMA field emission gun SEM equipped with an Everhart-Thornley detector operating in secondary electron detection mode, using 5 kV accelerating voltage, a 20 μm aperture, and 6.1 mm working distance. SEM images were analyzed using ImageJ, where roughness calculation plugin was used to calculate the root mean square of height deviation.[31]

2.5. X-ray photoelectron spectroscopy (XPS)

X-ray photoelectron spectroscopy (XPS) analysis was carried out using a Thermo Scientific ESCALAB 250 Xi system equipped with a monochromated Al Kα X-ray source with x-ray spot size 900 x 900 μm^2. Uniform charge neutralization was provided by multi-mode electrostatic flood source. Full survey scans (step size 1 eV, pass energy 150 eV, dwell time 50 ms and 5 scans) and narrow scans (step size 0.1 eV, pass energy 20 eV, dwell time 100 ms and 15 scans) of C1s (binding energy, BE ~285 eV), N1s (BE~400 eV) and O1s (BE~531 eV) were acquired from three separate regions from each sample. Data was analysed using Thermo Avantage Software (Version 5.952) using a smart background. XPS is a surface sensitive technique. Although x-rays penetrate deep into the surface under investigation, photoelectrons can only escape from not far below the surface. For polymers, XPS information depth is approximately 10nm; i.e. XPS characterizes the top 10nm surface layer of the sample under investigation. [32]

2.6. Four-point probe measurements.

Resistivity measurements were conducted on a 4-point probe system (Ossila Ltd, UK) using 3 points on each sample. Sheet resistance was measured with current of 10 μA and potential was recorded. Resistivity (ρ) was calculated as:

$$\rho = \frac{2\pi s \Delta V}{it}$$

where s is probe spacing (0.1 cm), ΔV is the potential change recorded, i is current sourced (10 μA) and t is the thickness is 3mm for the sensors.

2.7. Normalisation factors and data analysis

Eight different factors were used to normalise the current response observed on the 3D-printed electrodes. First was geometric surface area, calculated using the surface area of a circle to be 78.5 mm^2. Second was surface roughness, calculated using a roughness plugin on ImageJ. This plugin calculates variables in a similar approach to atomic force microscopy (AFM). The variable selected here for normalisation is the root mean square of height deviation (RMS height) which was computed in μm. [33] This was selected as it is a more sensitive measure of the inundations on the surface than average roughness as the root mean square includes squaring of the signal intensity calculated. [34] Third factor was oxygen functional groups, calculated by XPS. The fourth normalisation was the conductive load which was obtained from previously published work, which either collected the information from the supplier or measured it using thermal gravimetric analysis. [35, 36,37,38] The fifth factor was capacitance, which was measured through cyclic voltammetry response in 0.5 M KCl. The sixth factor was resistivity of the sensors measured by 4-point conductivity. Finally, the sixth and seventh normalisation factors were the current response from outer and inner sphere

standard redox probes. The current responses obtained from measurement of the three biological analytes were divided by the eight different normalisation factors to understand the influence it would have when comparing between the two different types of 3D-printed electrode. Data was shown as mean ± the standard deviation (SD). Statistical analysis (GraphPad Prism 7.0) using student t-tests and two-way ANOVA with Sidak *post hoc* tests were conducted to compare between the two electrodes.

3. Results

3.1. Normalisation Factors

The values obtained from the eight factors that were utilised to normalise the 3D-printed electrodes are shown in **Table 1.** These values relate the structure and conductive behaviour of the electrodes. The mean values for each electrode was used as the normalisation factor. The responses of the analytes measured were divided by these values.

There was no signficant difference in the geometric surface area between the two electrodes. The RMS of height, which was obtained through analysis of the SEM image, showed that the GR/PLA sensor was significantly rougher than the CB/PLA electrode ($n=3$, $p<0.01$, **Supplementary Figure 1**). Additionally, Energy Dispersive X-ray spectroscopy (EDS) measurements showed both electrodes contained trace metals. There was 0.1 % weight of Fe within the GR/PLA, whilst 0.1 % weight of both Mg and Al was present within the CB/PLA electrode (**Supplementary Figure 2**).

The oxygen functional group present on the electrode surface was obtained using XPS. The C-O-C, and O-C=O ($p<0.001$, $n=3$, **Supplementary Table 1**) are both significantly higher in GR/PLA in comparison to CB/PLA. Whilst the C=O was only

present in GR/PLA and N-C*=O was only present in CB/PLA, thus resulting in an overall significantly higher presence of oxygen functional groups in GR/PLA in comparison to CB/PLA ($p<0.001$, n=3, **Table 1**). The carbon content present within the filament was roughly double in the CB/PLA electrode when compared to the GR/PLA electrode.

The resistivity of the CB/PLA was significantly greater than that of the GR/PLA electrode ($p<0.001$, n=3, Table 1). However, the capacitance measured in 0.5 M KCl as shown in **Supplementary Figure 3** was significantly higher in GR/PLA when compared to the CB/PLA ($p<0.001$, n=3, **Table 1**). The current response obtained using CB/PLA and GR/PLA for the measurement of the outer sphere $Ru(NH_3)_6^{2+/3}$ (**Supplementary Figure 3**) and inner sphere $[Fe(CN)_6]^{2/3-}$ were not signficant different (n=3, **Table 1**).

Table 1: The different parameters utilised to normalise measurement of analytes. The mean values were utilised to normalise the current response of the 3D printed electrodes. Data shown as mean ± S.D., n=3, **p < 0.01 and ***p<0.001

Normalisation Factor	**CB / PLA**	**Graphene / PLA**
Geometric surface area (cm^2)	0.78	0.78
Root mean square average of height deviation (µm)	87 ± 2	197 ± 30**
Oxygen functional group content measured by XPS (%)	38 ± 1	60 ± 3***
Content of carbon material within the 3D printable filament (%)	22	10
Resistivity measurements conducted using 4-point probe (ohm)	5.0 ± 0.3	0.9 ± 0.3
Capacitive current from measurements using 0.5 M KCl (µF)	48 ± 10	299 ± 39

Faradaic outer sphere current from measurement of 1 mM $Ru(NH_3)_6^{2/3+}$ (µA)	-118 ± 24	-116 ± 45
Faradaic inner sphere current from measurement of 1 mM $[Fe(CN)_6]^{2/3-}$ (µA)	108 ± 32	102 ± 37

3.2. Normalisation of dopamine (DA) measurements

For DA, where representative cyclic voltammograms are displayed in **Figure 3A**, GR sensors showed significantly higher anodic current in comparison to CB (**Figure 3B,** $p<0.01$, n=3). A normalisation based upon the geometric area caused no change in this trend with GR sensors being significantly higher (**Figure 3C**, $p<0.01$, n=3). When normalising based on the RMS of height, no significant difference was found between the sensors (**Figure 3D**, n=3). Normalisation based on oxygen functional groups, computed by XPS, displayed a similar trend with no significant differences between the sensors (**Figure 3E**, n=3), while normalisation built on the conductive carbon content present in the GR/PLA and CB/PLA filaments displayed a significantly larger response for GR sensors in comparison to CB (**Figure 3F**, $p<0.001$, n=3). When comparing the resistivity, there was a significant increase in the GR sensor when compared to the CB electrode (**Figure 3G**, $p<0.001$, n=3). Normalisation based on the capacitive signal, showed a higher electrochemical performance for CB/PLA sensors in comparison to GR/PLA sensors (**Figure 3H**, $p<0.05$, n=3), while that based on faradaic outer sphere (OS) and inner sphere (IS) signal showed the opposite trend with GR/PLA being significantly higher than CB/PLA (**Figure 3I and J**, $p<0.01$, n=3).

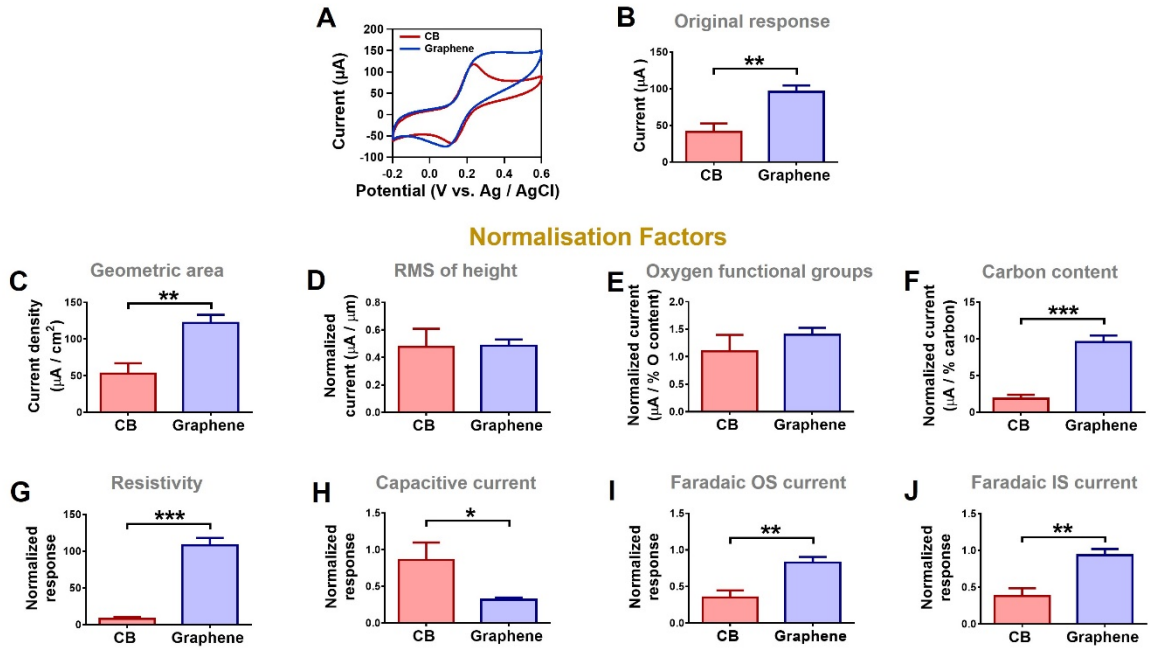

Figure 3. (A) Cyclic voltammograms of CB/PLA and GR/PLA (n=3) in 1 mM DA at 0.1 V s^{-1}. (B) Original anodic current and normalised anodic currents based on (C) geometric surface area, (D) RMS of height, (E) oxygen functional groups, (F) conductive carbon content, (G) resistivity, (H) capacitive current responses and (I) faradaic outer sphere (OS) current and (J) faradaic inner sphere (IS) current (n=3). Data shown as mean ± SD. All statistical comparisons were performed with student t-test *p<0.05, **p<0.01, ***p<0.001

3.3. Normalisation of ascorbic acid (AA) measurements

Representative cyclic voltammograms for AA (**Figure 4A**) and anodic current (**Figure 4B**) similarly show a significant difference in current between both sensors, with CB/PLA showing a higher response (p<0.01, n=3). When normalising based on geometric area a similar response is observed, with CB sensors showing a significantly higher current density (**Figure 4C,** p<0.01, n=3). RMS of height (**Figure 4D,** p<0.001, n=3), and oxygen functional groups (**Figure 4E,** p<0.001, n=3) normalisations result in a significantly larger current for CB/PLA sensors in comparison to GR/PLA sensors. This trend is reversed when normalising based on the conductive carbon content that results in the GR/PLA displaying a more enhanced performance

than the CB/PLA counterparts (**Figure 4F,** p<0.01, n=3). For resistivity normalisation, the GR/PLA responses was significantly higher than CB/PLA (**Figure 4G**, p<0.01, n=3). Capacitive current normalisations show CB/PLA sensors to be significantly higher (**Figure 4H,** p<0.001, n=3), while lastly, faradaic OS and IS current normalisation shows a similar trend with CB/PLA sensors having a significantly higher performance than GR/PLA (**Figure 4I and J,** p<0.05, n=3).

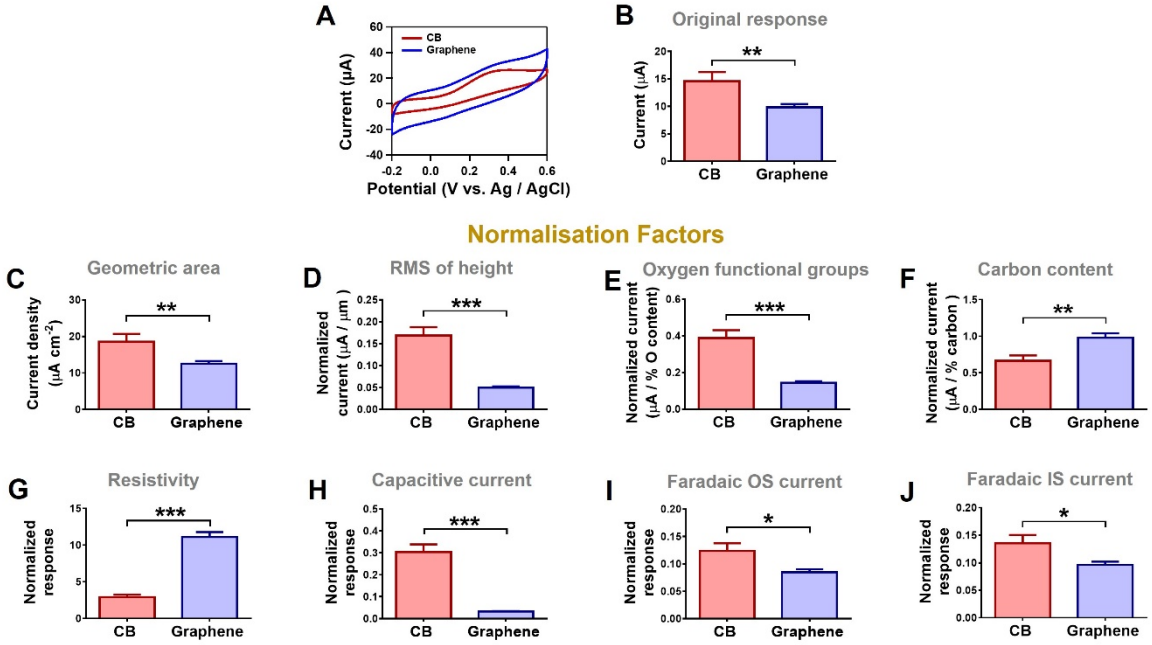

Figure 4. (A) Cyclic voltammograms of CB/PLA and GR/PLA (n=3) in 1 mM AA at 0.1 V s^{-1}. (B) Original anodic current and normalised anodic currents based on (C) geometric surface area, (D) RMS of height, (E) oxygen functional groups, (F) conductive carbon content, (G) resistivity, (H) capacitive current responses and (I) faradaic outer sphere (OS) current and (J) faradaic inner sphere (IS) current (n=3). Data shown as mean ± SD. All statistical comparisons were performed with student t-test *p<0.05, **p<0.01, ***p<0.0001.

3.4. Normalisation of calibration responses of hydrogen peroxide

For the measurement of H_2O_2, a calibration response was performed as is widely conducted as part of any electroanalytical study. Representative calibrations from 0.5 mM to 15 mM are displayed in **Figure 5A**. As can be seen in **Figure 5B**, the calibrations displayed a significantly higher response for GR/PLA at high

concentrations (7.5 mM, $p<0.05$; 10 mM, $p<0.01$; 15 mM, $p<0.001$, n=3). No change was seen to this trend when normalising based on the geometric area (**Figure 5C,** 7.5 mM, $p<0.05$; 10 mM, $p<0.01$; 15 mM, $p<0.001$, n=3). Normalising based on surface RMS of height enhanced the response of CB/PLA sensors at both low concentrations (2.5 mM, $p<0.01$, n=3) and a higher range of concentrations (5 – 15 mM, $p<0.001$, n=3) in comparison to GR/PLA sensors (**Figure 5D,** n=3). Similarly, as can be seen on **Figure 5E**, normalising based on oxygen functional groups showed a comparable trend for CB/PLA at both low concentrations (5mM, $p<0.05$, n=3) and higher range of concentrations (7.5 – 15 mM, $p<0.001$, n=3). The opposite trend in the calibrations can be seen upon normalising based on the conductive carbon content (**Figure 5F,** n=3), where GR/PLA sensors show a significantly higher calibration response both at low concentrations (2.5 mM, $p<0.05$, n=3) and a higher range of concentrations (5 – 15 mM, $p<0.001$). For resistivity normalisation, GR/PLA sensors show a significantly higher calibration response when compared to CB/PLA (**Figure 5G**, 2.5 mM, $p<0.01$; 5 – 15 mM, $p<0.001$ n=3). Capacitive current normalisation resulted in a significantly higher calibration response in the CB/PLA sensors at most concentrations (2.5 – 15mM, $p<0.001$, n=3) as can be seen in **Figure 5H**. Finally, the faradaic outer sphere and inner sphere current normalisation showed a similar trend to the raw current data, where only the higher concentrations in the GR/PLA calibration were significantly higher than CB/PLA calibration (**Figure 5I,** 7.5 mM, $p<0.05$; 10 mM, $p<0.01$; 15 mM, $p<0.001$, **Figure 5J,** 7.5 mM, $p<0.01$; 10 mM - 15 mM, $p<0.001$, n=3).

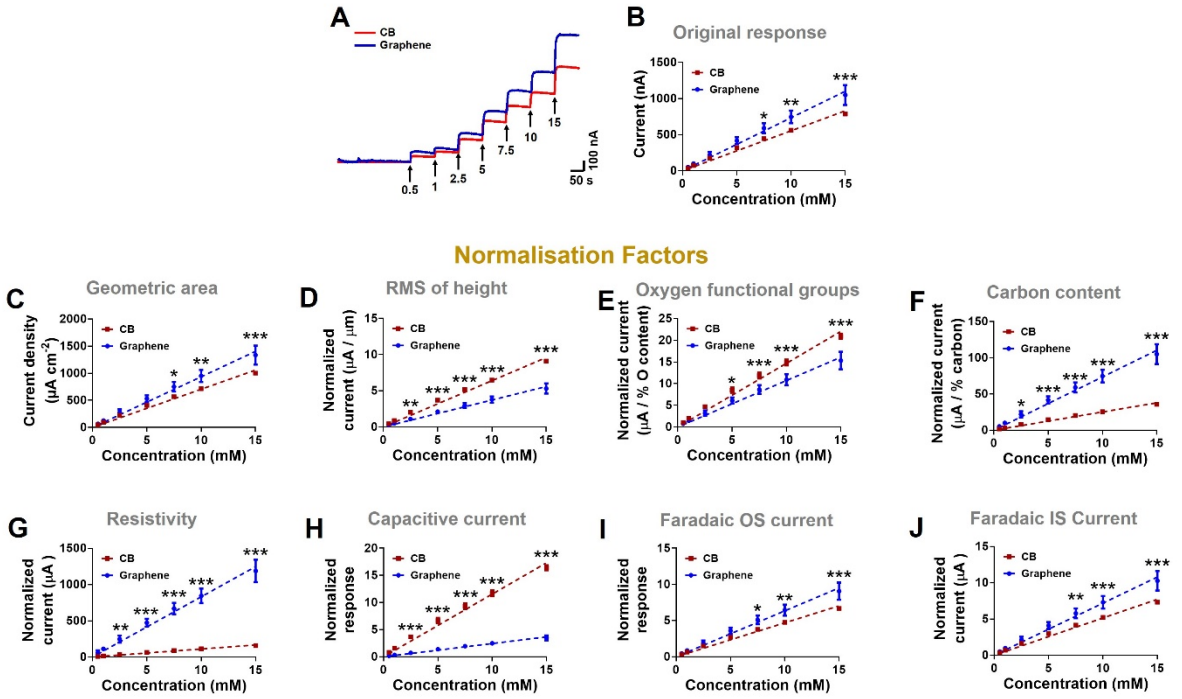

Figure 5. (A) Amperometric injections of hydrogen peroxide from 0.5 mM to 15mM every 100s on CB/PLA and GR/PLA sensors. (B) Original current calibrations on CB/PLA and GR/PLA sensors. Normalised anodic currents based on (C) geometric surface area, (D) RMS of height (E) oxygen functional groups (F) conductive carbon content (G) resistivity, (H) capacitive current responses and (I) faradaic outer sphere (OS) current and (J) faradaic inner sphere (IS) current (n=3). Data shown as mean ± SD. All statistical comparisons were performed with two-way ANOVA, *p<0.05, **p<0.01, ***p<0.0001.

4. Discussion

At present, CB/PLA and GR/PLA filaments are the most widely used in the manufacture of 3D-printed sensors for electroanalytical measurement. However, comparison between the two filaments or with other electrode materials poses challenges due to variation in the composition of the electrodes and surface geometry. Our study showcases normalising by eight different parameters can yield significantly different findings on the comparison between electrodes.

Based on SEM and ImageJ analysis, GR/PLA electrodes are rougher than CB/PLA electrodes. This is believed to be due to the printing process, where the high

temperatures cause moisture evaporation from the GR as it is thermally expanding. This results in the formation of voids along the surface which increases surface roughness. [39] This is further shown in the higher capacitance of GR/PLA, which could be a resultant of the rougher surface area.

The first normalisation parameter, and most widely used in comparison of sensors for electroanalytical measurements, is geometric surface area. In our case, the geometric area was the same for both sensors (0.785 cm^2) as the same dimensions and printing parameters were utilised. Thus, normalizing by this parameter, maintained the same trends seen on the raw data of both CB/PLA and GR/PLA sensors for the three molecules (current density - **Figures 3C, 4C & 5C**). This method of normalisation is effective when electrodes of distinctly varied geometry are being compared but assumes that the entire surface area is electroactive, which is not the case for 3D-printed sensors and therefore underestimates electrode performance.[40] This is more problematic when electrodes of different composition are compared. In addition, geometric area is not reflective of the microstructures, the pores, or the roughness of the surface at which electrochemical reactions occur and thus may be too simplified, especially in this case, where both sensors have identical geometric areas.

The second normalisation is based on RMS of height which is indicative of the surface roughness of the sensors as calculated through ImageJ processing of the SEM images. GR/PLA sensors were significantly rougher than their CB counterparts. For DA, normalisation based on surface roughness resulted in both sensors becoming comparative (**Figure 3D**), potentially suggestive then enhancement in the current may be due to the increased surface area. As a surface sensitive redox molecule, that is adsorptive in nature, the presence of edge versus basal planes is critical. GR sensors following pre-treatments are known to have more exposed edge planes[26] while CB

contains more basal planes. Thus, even though GR sensors were rougher the accessibility of these planes for DA adsorption and electron transfer becomes important. On the other hand, in both AA and H_2O_2, responses were significantly greater on the CB/PLA sensors (**Figures 4D and 5D**). Enhanced roughness on the GR/PLA electrode would suggest an increased surface area of the electrode, which should result in a bigger signal. However, after normalisation, this enhancement did not result in showcasing the enhanced performance of the electrode. Alternatively, this may be due to the potential bias of normalisation, as roughness may have little influence on electron transfer mechanisms[41-42]. The strength of this normalisation, contrary to geometric area, is that it considers the surface profile of the sensors more accurately, which is critical for 3D-printed electrodes, given that the printing parameters can have a drastic influence on the microstructure of the electrode surface. [24] However, even though it is a better indication of the surface area, this approach to normalisation does not differentiate between conductive and non-conductive components on the surface.

The next normalisation factor studied is the oxygen functional groups content as measured by XPS, where both sensors were comparable for DA (**Figure 3E)** but CB/PLA had significantly larger normalised currents for AA, and H_2O_2 (**4E & 5E**). As is well known for DA, even though it is not surface oxide sensitive, it is impacted by changes in other oxygen functional groups present on the surface, which hence makes this a promising parameter to normalize DA response with. AA on the other hand needs specific interactions with the carbon surface groups to either adsorb or anchor to make electron transfer possible. [43-44] This mechanism is yet to be determined and hence using this parameter may not ideal for this redox couple and could have led to a skew of the results in favour of CB. Finally, H_2O_2 exhibits improved electrochemical

responses over surfaces with rich oxygen functional groups, which could explain the higher response of anodic current for this redox couple on GR sesnosrs.[45-46] However, post normalisation, this trend was not the same. This could suggest that the source of these oxygen groups is trapped air in the voids, or that the oxygen functional groups present on GR are not all accessible for electrochemical reactions, perhaps due to the impurities on the surface or the higher surface roughness which would impede the catalytic reactions for H_2O_2. The use of this normalisation factor is advantageous when studying inner-sphere redox couples that are more dependent on surface oxygen chemistry. In addition, the ability to quantify the contribution of surface coverage from functional groups separately is useful when the molecule being studied is dependent on certain functional groups for anchoring or interaction, as well as quantification of how these percentages change post any form of sensor treatment. However, for XPS, it is critical that the electrodes are handled in the same manner, to avoid any false data due to different handling or storage of these sensors. Moreover, the presence of impurities or non-conductive elements to the sensor (such as PLA) with similar oxygen functional groups could lead to over estimation of the number of functional groups present on the surface. Finally, the presence of functional groups does not equate to available and functionally active surface groups during different experimental conditions.

The fourth normalisation factor is the amount of conductive carbon content present in the filaments. Previous work has shown that the carbon content in GR/PLA filament as per the supplier and TGA measurements is ~10% [35, 36] whereas TGA measurements on CB/PLA filaments show a ~22% carbon content [37,38]. Normalised measurements in DA, AA, and H_2O_2 show GR/PLA has a significantly larger normalised current response (**Figures 3F**, **4F**, and **5F**). This shows that although CB

filaments may contain more carbon content, this might not reflect on the electrochemical signal as the carbon would need to be present on the surface and accessible for electrochemical reactions, which might not be the case for CB sensors. Using this factor for normalisation has major advantages as it is reflective of the inherent electroactivity of the sensors whose main source is the carbon content, thus making it a good indicator of electrochemical performance. However, although it is important to know the amount of conductive content, this method does not shed light on the amount of conductive content present on the surface (homogeneity), or how much of it is accessible through conductive pathways throughout the material. In addition, this factor does not reflect on electrode surface geometry, which can have a signficant influence in the electrochemistry activity [41-42], or on the internal resistance caused by non-conductive parts of the sensor.

Resistivity was measured using 4-point probe and provides insight into the structure of the 3D printed materials and is an important measure of a 3D printed electrode, given that this is a composite electrode. For all analytes explored, the GR/PLA electrode has a significantly higher response than the CB/PLA electrode following normalisation (**Figures 3G**, **4G**, and **5G**). With the resistivity being much higher for CB/PLA electrodes than GR/PLA electrodes (Table 1), it is suggestive of a lower number of conductive pathways. Using this normalisation factor can be beneficial as it relates directly to the conductivity, given that it is the inverse of resistivity. Compared to carbon load, this provides understanding on which fraction of the carbon material is accessible for current flow and what fraction of that current load might have successfully formed conductive pathways throughout the printed material and thus is a more accurate measure of the electrode than just conductive load percentage. However, the limitation of this approach is on the ability to accurately measure this

component given that only regions of the electrode are monitored (3 regions) instead of the entire surface area of the electrode. However alternative strategies to measure the resistivity using conductive silver paint could be utilised to obtain punctual conductivity measurements at the cost of precision [47].

The subsequent normalisation factor investigated is capacitance. As can be seen from **Figures 3H**, **4H**, and **5H,** CB/PLA sensors show significantly higher normalised responses than GR/PLA based sensors. A higher percentage of oxygen functional groups on the surface layer has been previously linked to higher capacitance, as it helps in improving wettability and in the formation of double layer capacitance. [48-49] Thus, the higher amounts of oxygen functional groups seen by XPS in GR could further explain the larger capacitance in GR/PLA than CB/PLA. Furthermore, previous research into the pre-treatment of GR/PLA has shown that electrochemical pre-treatment of these electrodes leads to the exposure of GR/PLA edge planes along with increased surface oxygen functionalities as was presence of iron impurities, of which the latter may have a signficant influence the performance for peroxide determination.[26, 50-51] However, even though all these reasons explain why GR sensors may have higher capacitance, upon normalisation to this factor, the performance of CB sensors is seen to be larger for all 3 redox couples. This could be due to the process of normalisation itself, where dividing by this large capacitance cause GR sensors to become more impacted post normalisation. Alternatively, it could suggest that the CB/PLA sensors have a better signal-to-noise ratio. The use of capacitance as a normalisation factor is advantageous due to its selectivity to the conductive parts of the surface and can thus be used to understand how much of the surface is active. It is also a valuable tool for both solid and mesoporous structures, which is beneficial for 3D-printing sensors. On the other hand, capacitance

measurements need almost perfect replication between sensors, as any change in the electrode fabrication and storage, such as increased exposure to air, can cause huge variability in the capacitance measurements.

Finally, the last normalisation factors studied is based on faradaic current, in which we utilised both widely used outer sphere and inner sphere fully reversible redox couples. This mode of normalisation is one of the most widely used for sensors [22] due to the fact that measurement in ruthenium hexamine or ferricyanide is the preliminary step in the electrochemical characterisation of most sensors. This normalisation shows an identical trend to the raw currents since both sensors had almost identical responses to ruthenium hexamine and ferricyanide. Although these redox probes are widely used, it is assumed when using them that the surface interactions of the analytes measured are similar to those redox probes, however the electron transfer mechanism of all three biological analytes is actually different, although they are all inner sphere redox probes similar to ferricyanide. This can be a limitation on the accuracy of this normalisation approach compared to capacitance normalisation, which just provides insight into the active electrode surface area.

Different normalisation factors, each with their own strengths and weaknesses allow for a better examination and comparison between the two different composite 3D-printed filaments. This list is not comprehensive, as depending on the sensors being studied and the molecules that need to be monitored, different normalisation factors may need to be employed. This is especially important when utilizing composite 3D-printed materials that are not fully conductive or smooth, but rough, with voids and pores and a mix of conductive and non-conductive components. Additionally, what is critical to note, is that depending on the monitored molecule and its mode of action, some normalisation factors may result in skewing of the result if they are not reflective

of this molecule's electron transfer reaction mechanism. However, if the trend observed for one electrode using multiple appropriate normalisation factors showcases superior performance than another, then greater confidence can be achieved when choosing the best sensor for electroanalysis.

5. Conclusion

The use of 3D-printed electrodes in an analytical setting can be highly advantageous due to the ability of 3D printers to mass produce robust conductive parts of complex geometries, both quickly and inexpensively. In this study we showed that sensors fabricated from the two most common 3D-printing filaments, CB/PLA and GR/PLA, on face value have different electrochemical performances in DA, AA and H_2O_2. However, when these responses are normalised based on the geometric area, root mean square deviation in height, oxygen functional groups, capacitance, carbon content, resistivity and faradaic inner and outer sphere current differences between the electrochemical performance of these sensors becomes more apparent. This study highlights the importance of examining different methods of normalisation to compare between different 3D-printed electrodes to study their potential as better sensing devices for different biological molecules. It showcases that no one single normalisation factor can be used in its own when comparing complex composite 3D-printed sensors and that it is critically important to study first the redox molecules and how they interact with the surface to determine the ideal set of normalisation parameters.

Acknowledgements

Authors would like to acknowledge Dr.Jon Salvage for experimental assistance on conducting SEM studies.

Funding

F.P would like to thank EPSRC studentship for funding. A.T would like to thank DTA3/COFUND Marie Skłodowska-Curie PhD Fellowship programme for funding. Studies were funded by and IMPRESSPlus EPSRC grant (EP/N027345/1) awarded to B.A.P.

Conflict of Interest

The authors declare no conflict of interest

References

1. Kwok, S. W.; Goh, K. H. H.; Tan, Z. D.; Tan, S. T. M.; Tjiu, W. W.; Soh, J. Y.; Ng, Z. J. G.; Chan, Y. Z.; Hui, H. K.; Goh, K. E. J., Electrically conductive filament for 3D-printed circuits and sensors. *Applied Materials Today* **2017,** *9*, 167-175.
2. Lee, J.-Y.; An, J.; Chua, C. K., Fundamentals and applications of 3D printing for novel materials. *Applied Materials Today* **2017,** *7*, 120-133.
3. Ambrosi, A.; Pumera, M., 3D-printing technologies for electrochemical applications. *Chem. Soc. Rev.* **2016,** *45*, 2740.
4. Manzanares Palenzuela, C. L.; Pumera, M., (Bio)Analytical chemistry enabled by 3D printing: Sensors and biosensors. *TrAC Trends in Analytical Chemistry* **2018,** *103*, 110-118.
5. Hamzah, H. H.; Shafiee, S. A.; Abdalla, A.; Patel, B. A., 3D printable conductive materials for the fabrication of electrochemical sensors: A mini review. *Electrochemistry Communications* **2018**.
6. Ngo, T. D.; Kashani, A.; Imbalzano, G.; Nguyen, K. T. Q.; Hui, D., Additive manufacturing (3D printing): A review of materials, methods, applications and challenges. *Composites Part B: Engineering* **2018,** *143*, 172-196.
7. Gross, B.; Lockwood, S. Y.; Spence, D. M., Recent Advances in Analytical Chemistry by 3D Printing. *Analytical Chemistry* **2017,** *89* (1), 57-70.
8. Hamzah, H. H. B.; Keattch, O.; Covill, D.; Patel, B. A., The effects of printing orientation on the electrochemical behaviour of 3D printed acrylonitrile butadiene styrene (ABS)/carbon black electrodes. *Scientific Reports* **2018,** *8* (1), 9135.
9. Rymansaib, Z.; Iravani, P.; Emslie, E.; Medvidović-Kosanović, M.; Sak-Bosnar, M.; Verdejo, R.; Marken, F., All-Polystyrene 3D-Printed Electrochemical Device with Embedded Carbon Nanofiber-Graphite-Polystyrene Composite Conductor. *Electroanalysis* **2016,** *28*, 1517.

10. Honeychurch, K. C.; Rymansaib, Z.; Iravani, P., Anodic stripping voltammetric determination of zinc at a 3-D printed carbon nanofiber–graphite–polystyrene electrode using a carbon pseudo-reference electrode. *Sensors and Actuators B: Chemical* **2018,** *267*, 476-482.
11. Browne, M. P.; Novotný, F.; Sofer, Z.; Pumera, M., 3D Printed Graphene Electrodes' Electrochemical Activation. *ACS Applied Materials & Interfaces* **2018,** *10* (46), 40294-40301.
12. Foster, C. W.; Down, M. P.; Zhang, Y.; Ji, X. B.; Rowley-Neale, S. J.; Smith, G. C.; Kelly, P. J.; Banks, C. E., 3D Printed Graphene Based Energy Storage Devices. *Sci. Rep.* **2017,** *7*, 42233.
13. Manzanares Palenzuela, C. L.; Novotný, F.; Krupička, P.; Sofer, Z.; Pumera, M., 3D-Printed Graphene/Polylactic Acid Electrodes Promise High Sensitivity in Electroanalysis. *Analytical Chemistry* **2018,** *90* (9), 5753-5757.
14. O'Neil, G. D.; Ahmed, S.; Halloran, K.; Janusz, J. N.; Rodríguez, A.; Terrero Rodríguez, I. M., Single-step fabrication of electrochemical flow cells utilizing multi-material 3D printing. *Electrochemistry Communications* **2019,** *99*, 56-60.
15. Cardoso, R. M.; Mendonça, D. M. H.; Silva, W. P.; Silva, M. N. T.; Nossol, E.; da Silva, R. A. B.; Richter, E. M.; Muñoz, R. A. A., 3D printing for electroanalysis: From multiuse electrochemical cells to sensors. *Analytica Chimica Acta* **2018,** *1033*, 49-57.
16. Leigh, S. J.; Bradley, R. J.; Purssell, C. P.; Billson, D. R.; Hutchins, D. A., A Simple, Low-Cost Conductive Composite Material for 3D Printing of Electronic Sensors. *PLoS One* **2012,** *7* (11), e49365.
17. Postiglione, G.; Natale, G.; Griffini, G.; Levi, M.; Turri, S., Conductive 3D microstructures by direct 3D printing of polymer/carbon nanotube nanocomposites via liquid deposition modeling. *Composites Part A: Applied Science and Manufacturing* **2015,** *76*, 110-114.
18. Cruz, M. A.; Ye, S.; Kim, M. J.; Reyes, C.; Yang, F.; Flowers, P. F.; Wiley, B. J., Multigram Synthesis of Cu-Ag Core–Shell Nanowires Enables the Production of a Highly Conductive Polymer Filament for 3D Printing Electronics. *Particle & Particle Systems Characterization* **2018,** *35* (5), 1700385.
19. Ren, H.; Pan, Y.; Sorrell, C. C.; Du, H., Assessment of electrocatalytic activity through the lens of three surface area normalization techniques. *Journal of Materials Chemistry A* **2020,** *8* (6), 3154-3159.
20. Clark, E. L.; Resasco, J.; Landers, A.; Lin, J.; Chung, L.-T.; Walton, A.; Hahn, C.; Jaramillo, T. F.; Bell, A. T., Standards and Protocols for Data Acquisition and Reporting for Studies of the Electrochemical Reduction of Carbon Dioxide. *ACS Catalysis* **2018,** *8* (7), 6560-6570.
21. Sun, S.; Li, H.; Xu, Z. J., Impact of Surface Area in Evaluation of Catalyst Activity. *Joule* **2018,** *2* (6), 1024-1027.
22. Patel, N.; Fagan-Murphy, A.; Covill, D.; Patel, B. A., 3D Printed Molds Encompassing Carbon Composite Electrodes To Conduct Multisite Monitoring in the Entire Colon. *Analytical Chemistry* **2017,** *89* (21), 11690-11696.
23. Noorani, R., *3D printing: technology, applications, and selection*. CRC Press: 2017.
24. Bin Hamzah, H. H.; Keattch, O.; Covill, D.; Patel, B. A., The effects of printing orientation on the electrochemical behaviour of 3D printed acrylonitrile butadiene styrene (ABS)/carbon black electrodes. *Scientific Reports* **2018,** *8* (1), 9135.
25. Abdalla, A.; Hamzah, H. H.; Keattch, O.; Covill, D.; Patel, B. A., Augmentation of conductive pathways in carbon black/PLA 3D-printed electrodes achieved through varying printing parameters. *Electrochimica Acta* **2020**, 136618.
26. dos Santos, P. L.; Katic, V.; Loureiro, H. C.; dos Santos, M. F.; dos Santos, D. P.; Formiga, A. L. B.; Bonacin, J. A., Enhanced performance of 3D printed graphene electrodes after electrochemical pre-treatment: Role of exposed graphene sheets. *Sensors and Actuators B: Chemical* **2019,** *281*, 837-848.
27. Katic, V.; dos Santos, P. L.; dos Santos, M. F.; Pires, B. M.; Loureiro, H. C.; Lima, A. P.; Queiroz, J. C. M.; Landers, R.; Muñoz, R. A. A.; Bonacin, J. A., 3D Printed Graphene Electrodes Modified with Prussian Blue: Emerging Electrochemical Sensing Platform for Peroxide Detection. *ACS Applied Materials & Interfaces* **2019,** *11* (38), 35068-35078.

28. Richter, E. M.; Rocha, D. P.; Cardoso, R. M.; Keefe, E. M.; Foster, C. W.; Munoz, R. A. A.; Banks, C. E., Complete Additively Manufactured (3D-Printed) Electrochemical Sensing Platform. *Analytical Chemistry* **2019,** *91* (20), 12844-12851.
29. Kalinke, C.; Neumsteir, N. V.; Aparecido, G. d. O.; Ferraz, T. V. d. B.; dos Santos, P. L.; Janegitz, B. C.; Bonacin, J. A., Comparison of activation processes for 3D printed PLA-graphene electrodes: electrochemical properties and application for sensing of dopamine. *Analyst* **2020,** *145* (4), 1207-1218.
30. Klunder, K. J.; Nilsson, Z.; Sambur, J. B.; Henry, C. S., Patternable Solvent-Processed Thermoplastic Graphite Electrodes. *Journal of the American Chemical Society* **2017,** *139* (36), 12623-12631.
31. Gary Chinga, B. D. Roughness calculation. https://imagej.nih.gov/ij/plugins/roughness.html (accessed 03/06/2020).
32. Briggs, D.; Seah, M. P., *Practical surface analysis : by auger and x-ray photoelectron spectroscopy*. Wiley: Chichester ; New York, 1983; p xiv, 533 p.
33. Jumelle, C.; Hamri, A.; Egaud, G.; Mauclair, C.; Reynaud, S.; Dumas, V.; Pereira, S.; Garcin, T.; Gain, P.; Thuret, G., Comparison of four methods of surface roughness assessment of corneal stromal bed after lamellar cutting. *Biomed Opt Express* **2017,** *8* (11), 4974-4986.
34. Oliveira, R. A. d.; Albuquerque, D.; Cruz, T.; Yamaji, F. M.; Leite, F. L. In *Measurement of the Nanoscale Roughness by Atomic Force Microscopy: Basic Principles and Applications*, 2012.
35. Foster, C. W.; Down, M. P.; Zhang, Y.; Ji, X.; Rowley-Neale, S. J.; Smith, G. C.; Kelly, P. J.; Banks, C. E., 3D Printed Graphene Based Energy Storage Devices. *Scientific Reports* **2017,** *7* (1), 42233.
36. Paddubskaya, A.; Valynets, N.; Kuzhir, P.; Batrakov, K.; Maksimenko, S.; Kotsilkova, R.; Velichkova, H.; Petrova, I.; Biró, I.; Kertész, K.; Márk, G. I.; Horváth, Z. E.; Biró, L. P., Electromagnetic and thermal properties of three-dimensional printed multilayered nano-carbon/poly(lactic) acid structures. *Journal of Applied Physics* **2016,** *119* (13), 135102.
37. Kim, H.; Lee, S., Characterization of Electrical Heating of Graphene/PLA Honeycomb Structure Composite Manufactured by CFDM 3D Printer. *Fashion and Textiles* **2020,** *7* (1), 8.
38. Jaksic, N. I.; Desai, P. D., Characterization of 3D-printed capacitors created by fused filament fabrication using electrically-conductive filament. *Procedia Manufacturing* **2019,** *38*, 33-41.
39. Gnanasekaran, K.; Heijmans, T.; van Bennekom, S.; Woldhuis, H.; Wijnia, S.; de With, G.; Friedrich, H., 3D printing of CNT- and graphene-based conductive polymer nanocomposites by fused deposition modeling. *Applied Materials Today* **2017,** *9*, 21-28.
40. Clark, E. L.; Resasco, J.; Landers, A.; Lin, J.; Chung, L.-T.; Walton, A.; Hahn, C.; Jaramillo, T. F.; Bell, A. T., Standards and Protocols for Data Acquisition and Reporting for Studies of the Electrochemical Reduction of Carbon Dioxide. *ACS Catalysis* **2018**, Medium: ED; Size: p. 6560-6570.
41. Paixão, T. R. L. C., Measuring Electrochemical Surface Area of Nanomaterials versus the Randles−Ševčík Equation. *ChemElectroChem* **2020,** *7* (16), 3414-3415.
42. Li, D.; Batchelor-McAuley, C.; Compton, R. G., Some thoughts about reporting the electrocatalytic performance of nanomaterials. *Applied Materials Today* **2020,** *18*, 100404.
43. Hu, I. F.; Kuwana, T., Oxidative mechanism of ascorbic acid at glassy carbon electrodes. *Analytical Chemistry* **1986,** *58* (14), 3235-3239.
44. Fagan, D. T.; Hu, I. F.; Kuwana, T., Vacuum heat-treatment for activation of glassy carbon electrodes. *Analytical Chemistry* **1985,** *57* (14), 2759-2763.
45. Halliwell, B.; Clement, M. V.; Long, L. H., Hydrogen peroxide in the human body. *FEBS Letters* **2000,** *486* (1), 10-13.
46. Lu, Z.; Chen, G.; Siahrostami, S.; Chen, Z.; Liu, K.; Xie, J.; Liao, L.; Wu, T.; Lin, D.; Liu, Y.; Jaramillo, T. F.; Nørskov, J. K.; Cui, Y., High-efficiency oxygen reduction to hydrogen peroxide catalysed by oxidized carbon materials. *Nature Catalysis* **2018,** *1* (2), 156-162.
47. Meloni, G. N.; Bertotti, M., 3D printing scanning electron microscopy sample holders: A quick and cost effective alternative for custom holder fabrication. *PloS one* **2017,** *12* (7), e0182000-e0182000.

48. Shrestha, S.; Morse, N.; Mustain, W. E., Effect of surface chemistry on the double layer capacitance of polypyrrole-derived ordered mesoporous carbon. *RSC Advances* **2014,** *4* (87), 47039-47046.
49. Yamashita, A.; Minoura, S.; Miyake, T.; Ikenaga, N.; Oda, H., Modification of functional groups on ACF surface and its application to electric double layer capacitor electrode. *TANSO* **2004,** *2004*, 194-201.
50. Browne, M. P.; Pumera, M., Impurities in graphene/PLA 3D-printing filaments dramatically influence the electrochemical properties of the devices. *Chemical Communications* **2019,** *55* (58), 8374-8377.
51. Rocha, R. G.; Stefano, J. S.; Cardoso, R. M.; Zambiazi, P. J.; Bonacin, J. A.; Richter, E. M.; Munoz, R. A. A., Electrochemical synthesis of Prussian blue from iron impurities in 3D-printed graphene electrodes: Amperometric sensing platform for hydrogen peroxide. *Talanta* **2020,** *219*, 121289.

Supporting Information

How Normalisation Factors Influence the Interpretations of 3D-Printed Sensors for Electroanalysis

Aya Abdalla[1, 2], Fernando Perez[1, 2], Ana Tendero Cañadas[1, 2], Santanu Ray[3] and Bhavik Anil Patel[1, 2*]

[1]School of Pharmacy and Biomolecular Sciences, [2]Centre for Stress and Age-Related Disease and [3]Surface Analysis Laboratory, School of Environment and Technology, University of Brighton, Brighton, East Sussex, UK

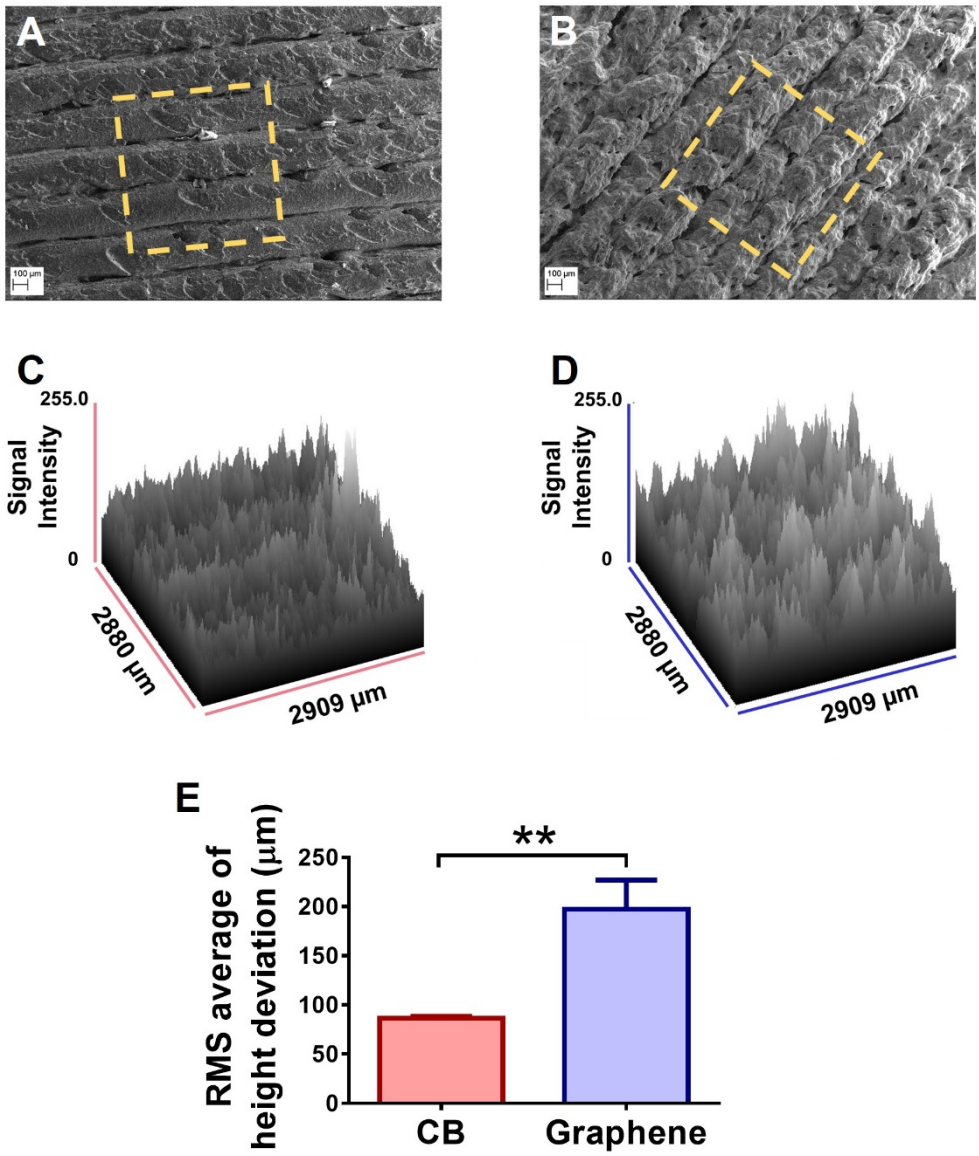

Supplementary Figure 1: SEM images of (A) CB/PLA sensors and (B) GR/PLA sensors where yellow squares denote area used to generate surface plots for (C) CB/PLA and (D) GR/PLA using Image J. (E) Root mean square of height deviation for GR/PLA was significantly greater than that for CB/PLA. Data shown as mean ± SD, where **p<0.01 (student t-test).

Supplementary Table 1: Differences between C1s functional groups in CB/PLA and GR/PLA. Data shown as mean ± SD. All statistical comparisons were performed with student t-test. (n=3 areas) ***p<0.001

Oxygen functional groups	**CB / PLA (%)**	**Graphene / PLA (%)**
C1s C*-O-C	20.6 ± 1.6	31.0 ± 2.1***
C1s C*=O	n/a	8.7 ± 6.3
C1s O-C*=O	9.5 ± 0.3	19.8 ± 1.6***
C1s N-C*=O	7.6 ± 0.4	n/a
Total oxygen functional groups	**37.7 ± 1.2**	**59.5 ± 2.9*** **

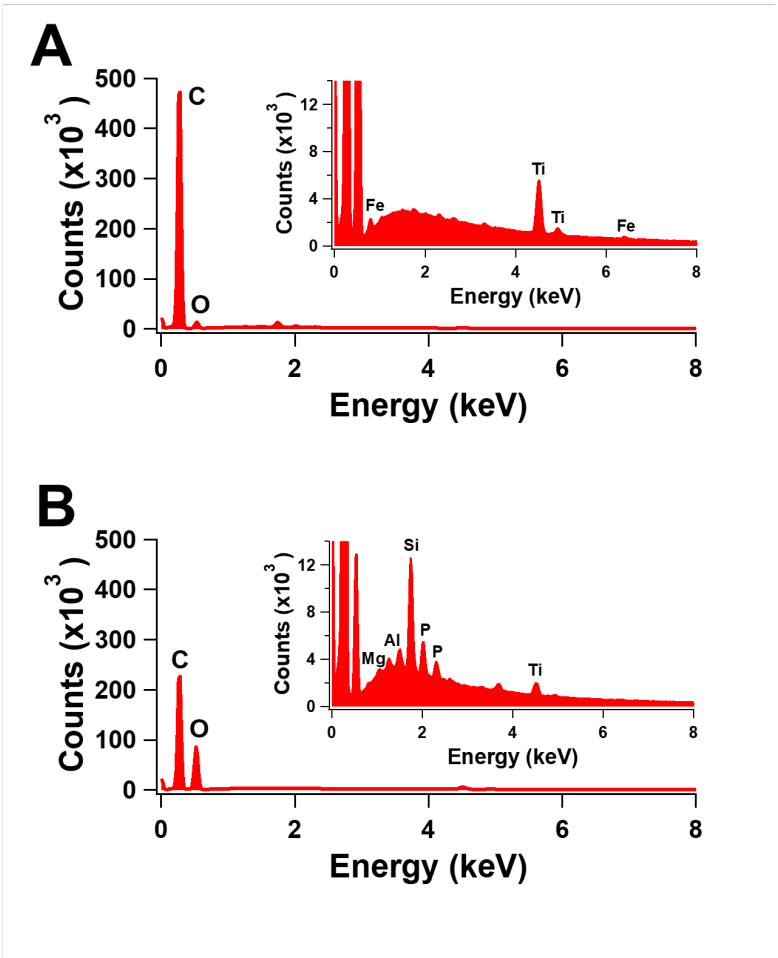

Supplementary Figure 2: EDS spectra of CB/PLA and GR/PLA electrodes.

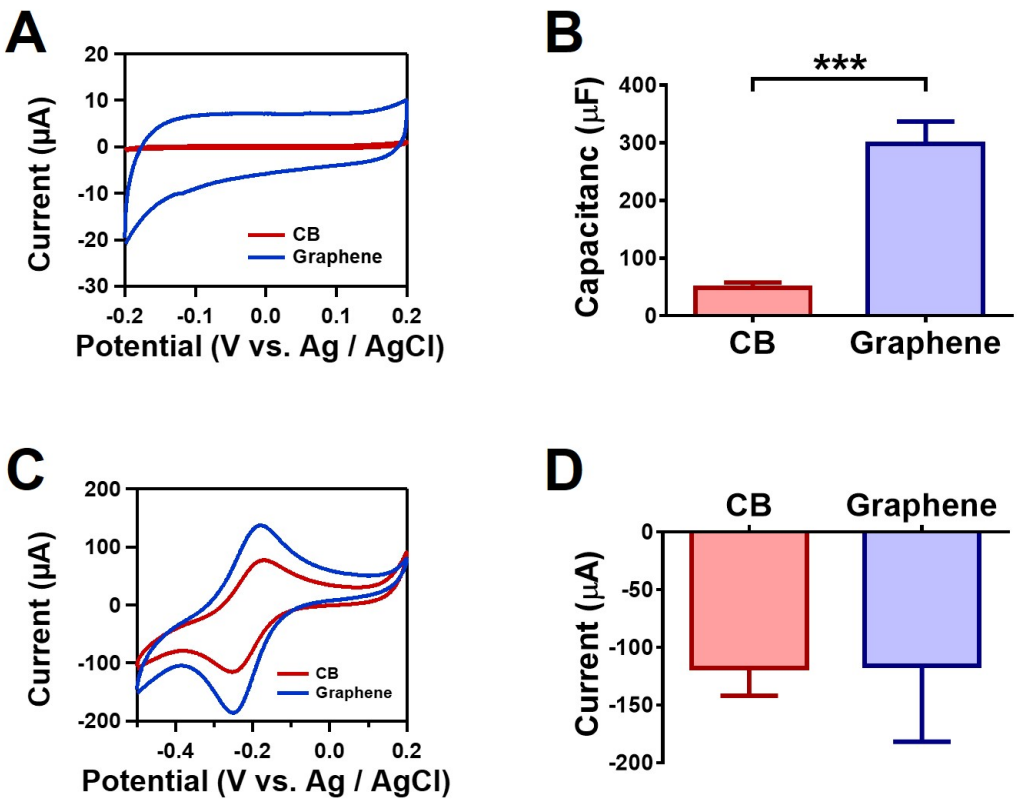

Supplementary Figure 3: Representative cyclic voltammograms signals of CB/PLA and GR/PLA sensors in (A) 0.5 M KCl and (C) 1 mM $Ru(NH_3)_6^{2+/3}$ at 0.1 V s^{-1}. (B) Capacitance (µF) and (D) Cathodic current (µA) in 1 mM $Ru(NH_3)_6^{2+/3}$ at 0.1 V s^{-1} for CB/PLA and GR/PLA. Data shown as mean ± SD, where ***p<0.001 (student t-test).